Inorganic Chemistry

Article

pubs.acs.org/IC

$ThPt_2$: A New Representative of Close Packed Tetragonal Structures

Roman Gumeniuk,*[,†,‡] Walter Schnelle,[†] Ulrich Burkhardt,[†] Horst Borrmann,[†] Michael Nicklas,[†] Alim Ormeci,[†] Miroslav Kohout,[†] Andreas Leithe-Jasper,[†] and Yuri Grin[†]

[†]Max-Planck-Institut für Chemische Physik fester Stoffe, Nöthnitzer Straße 40, 01187 Dresden, Germany

[‡]Institut für Experimentelle Physik, TU Bergakademie Freiberg, Leipziger Straße 23, 09596 Freiberg, Germany

ABSTRACT: $ThPt_2$ crystallizes with unique type of structure (space group *I*4/*mmm*, *a* = 4.1565(1) Å, *c* = 14.3663(7) Å, Pearson symbol *tI*12), which belongs to the group of the close packed tetragonal structures. An analysis of the chemical bonding by the electron localizability approach reveals the formation of two-dimensional layered platinum anionic substructures interlinked by strongly polar bonds to Th. Measurements of magnetic susceptibility, electrical resistivity, and specific heat show $ThPt_2$ to be diamagnetic with metallic type of electrical conductivity in good agreement with the calculated electronic structure ($N(E_F)$ = 0.9 states eV^{-1} f.u.$^{-1}$).

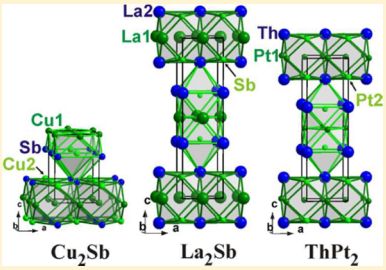

INTRODUCTION

Laves phases are intermetallic compounds with a common composition AB_2 and tetrahedrally close packed structures, where atoms show a size ratio of $(3/2)^{1/2} \approx 1.225$.[1,2] The typically observed polytypes for such structural arrangements are cubic *C*15 ($MgCu_2$) as well as hexagonal *C*14 ($MgZn_2$) and *C*36 ($MgNi_2$).[3] More than 350 binary Laves phases are known to exist so far.[4] They are of particular interest due to their potential practical applications. The most exciting properties of some Laves phases are retention of mechanical properties at elevated temperatures (ACr_2-based alloys), superconductivity with relatively high critical temperatures ($(Hf, Zr)V_2$), strong magnetostriction ($(Tb,Dy)Fe_2$), application as hydrogen storage materials ($Zr(Cr,Fe)_2$), etc.[5] Actinide-containing Laves phases attract more attention due to the dual nature of the 5f electronic states, which in contrary to the 4f electrons show both localized and itinerant behavior and thus a wealth of topical physical properties. A delocalized picture of the 5f electrons is reported for UM_2 (M = Mn, Fe, Co, and Ni) cubic Laves systems.[6] Very high density of states at the Fermi level, which appears as an extremely narrow band feature, gives rise to the spin fluctuations observed in UAl_2.[7] $ThRu_2$, $ThOs_2$, and $ThIr_2$ are reported to crystallize with the cubic $MgCu_2$ type of crystal structure.[8] $ThRu_2$ and $ThIr_2$ are superconductors with critical temperatures of 3.7 and 6.5 K, respectively.[9] The compound $ThPt_2$ with a hitherto unknown crystal structure is of special interest in this respect.[10]

The first compound which was discovered by Thomson in the Th−Pt system was Th_7Pt_3.[11] A few years later the same author reported crystal structures of ThPt (CrB type)[12] and Th_3Pt_5 (Th_3Pd_5 type) compounds.[13] The phase diagram of the Th−Pt binary system was published in 1964[14] and then evaluated by Peterson in 1990.[15] The system is characterized by the presence of eight intermetallic compounds: ThPt, Th_3Pt_5, and $ThPt_3$, which melt congruently, and Th_7Pt_3, Th_3Pt_4, $ThPt_2$, $ThPt_4$, and $ThPt_5$, which form by peritectic reactions. $ThPt_5$ was later reported to crystallize with the $SmPt_5$ type of structure,[16] while no crystallographic data for Th_3Pt_4, $ThPt_2$, $ThPt_3$, or $ThPt_4$ are available in the literature up to now. Further investigations showed Th_7Pt_3, ThPt, and $ThPt_5$ to be superconducting with T_c of 0.98 K, 0.44 K, and 3.13 K, respectively.[17] Metallic behavior of electrical resistivity is observed for ThPt in the temperature range 1.5−300 K.[18] In order to determine the positions and intensities of the 5f electron states in the respective U−Pt compounds, X-ray photoelectron spectra were measured. In the course of these investigations the electron binding energies of selected core levels and work functions for ThPt, $ThPt_2$, and $ThPt_3$ were estimated.[10]

In this paper we report on the crystal structure, electronic structure, chemical bonding, and physical properties of $ThPt_2$.

EXPERIMENTAL SECTION

The precursor samples with the molar ratios Th:Pt of 1:2 were prepared by arc melting of the elements Th (Goodfellow, 99.5 mass % of metal base and 2 mass % of ThO_2) and Pt (ChemPur, 99.9 wt %). The resulting ingots were placed in ZrO_2 crucibles, sealed in tantalum tubes, and annealed at 1400 °C for 48 h and 1000 °C for 2 weeks. Sample handling was performed in argon-filled glove boxes (MBraun, $p(H_2O)$ < 1 ppm; $p(O_2)$ < 1 ppm).

For metallographic investigations, a polished cut of the $ThPt_2$ sample was examined by energy-dispersive X-ray spectroscopy (EDXS) using a Jeol JSM 6610 scanning electron microscope equipped with an UltraDry EDXS detector (ThermoFisher NSS7 system). The element mapping based on the X-ray intensities of Th *M*, Pt *M*, and O *K* lines shows the presence of $ThPt_2$ as well as ThO_2 and $ThPt_3$ minority phases (Figure 1). The semiquantitative EDXS analyses were performed with 30 keV acceleration voltage and approximately 3 nA beam current. The $\varphi(\rho z)$ matrix correction model was applied to calculate the compositions from the intensities of Th *M* and Pt *L* lines. No oxygen O *K* line was observed in the phases containing both Th and Pt.

Received: March 24, 2015
Published: June 23, 2015

DOI: 10.1021/acs.inorgchem.5b00669
Inorg. Chem. 2015, 54, 6338−6346

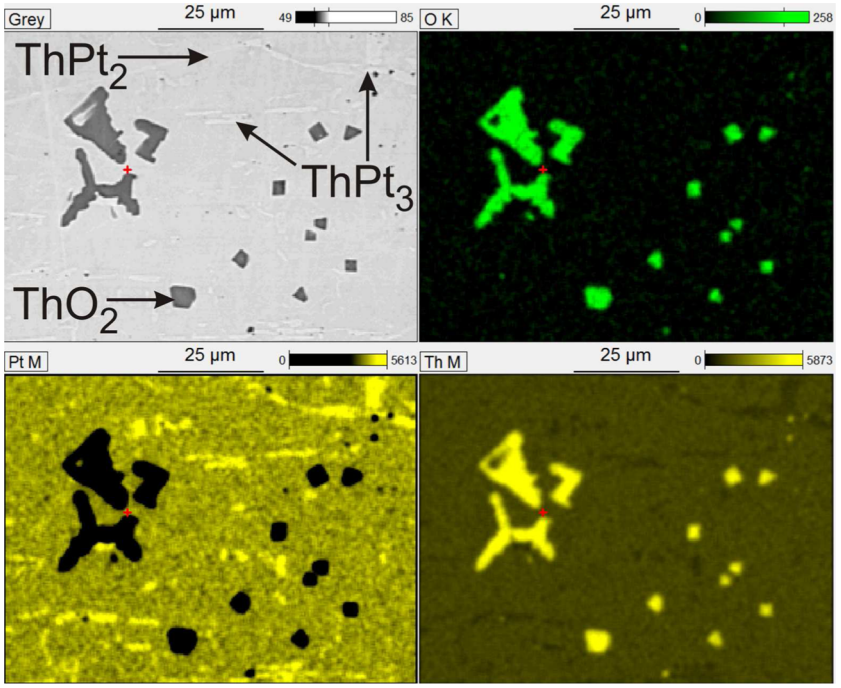

Figure 1. Microstructure and element distribution in the synthesized $ThPt_2$ sample. X-ray intensity element mappings show the EDXS net counts of Th *M*, Pt *M*, and O *K* lines. The minority phases ThO_2 and $ThPt_3$ are labeled in back scattered electron image (upper left).

Powder X-ray diffraction (PXRD) of the products was performed on a HUBER G670 imaging plate Guinier camera with Cu $K\alpha_1$ radiation (λ = 1.540598 Å). The *WinXPow* program package[19] was used to carry out the phase identification as well as for automatic indexing of peaks of unknown phases with the algorithm TREOR. Lattice parameter refinement by least-squares fitting, crystal structure solution from X-ray powder diffraction pattern, and refinement have been done using the program package *WinCSD*.[20]

All preparation and characterization operations were performed in a dedicated laboratory with high safety standard at the MPI CPfS.[21]

The scalar-relativistic electronic structure of all compounds was calculated in the framework of density-functional theory (DFT) using the TB-LMTO-ASA[22] or the full-potential FPLO code (version 9.01-35) with the basis set of local orbitals.[23] The exchange-correlation potential by Perdew and Wang was applied.[24] The *k* meshes included 641 points for $ThPt_2$, 163 points for hypothetic Th_2Pt_4O, and 256 points for ThT_2 (T = Os, Ir, Pt; $MgCu_2$ type of crystal structure) in the symmetry-irreducible part of the first Brillouin zone. The highest-lying valence states do not show any significant spin−orbit coupling driven effects; therefore our presentation here is confined to the results of the scalar relativistic calculations. In the LMTO calculations for MPt_2 (M = Na, Sr, Ba, Y, La Ce, Hf), the basis sets containing Na(3s), Sr(5s, 4d), Ba(6s, 5d, 4f), Y(5s, 4d), La(6s, 5d, 4f), Ce(6s, 5d, 4f), Hf (6s, 6p, 5d), and Pt (6s, 6p, 5d) orbitals were employed with Na(3p, 3d), Sr(5p), Ba(6p), Y(5p), La(6p), Ce(6p), Hf (5f), and Pt (5f) functions being down folded.

The electron localizability indicator (ELI, Υ)[25] was evaluated in the ELI-D representation according to refs 25 and 26 with ELI modules within the TB-LMTO-ASA[22] and FPLO[23] program packages. The topology of the electron density and ELI-D obtained from the LMTO-ASA and FPLO calculations was evaluated with the program DGrid[27] and was found to be practically identical.

To compare XPS spectra, reported for $ThPt_2$ in ref 10, with our theoretical calculations, partial DOS of all atoms contributing to the valence band were multiplied by the corresponding weight factors proportional to the atomic subshell photoionization cross sections.[28] The outputs were summed and multiplied by the Fermi−Dirac function for 300 K and convoluted with a Lorentzian (full width of half-maximum of 1.1 eV) to obtain the instrumental energy resolution of the analyzer used in the experiment.[29]

The magnetization of polycrystalline sample was measured in a SQUID magnetometer (MPMS XL-7, Quantum Design) in external fields $\mu_0 H$ between 2 mT and 7 T and temperatures between 1.8−400 K. The heat capacity measurements were performed with a relaxation-type calorimeter (PPMS, Quantum Design) in magnetic fields up to 9 T between 1.8 and 320 K. Electrical resistivity was determined with a low-frequency ac technique on a PPMS platform in zero and 9 T fields. The resistivity down to 0.35 K was measured on a PPMS (Quantum Design) with ^{3}He option.

RESULTS AND DISCUSSION

Crystal Structure Determination. The 34 strongest reflections of the powder XRD pattern of $ThPt_2$ were successfully indexed assuming a tetragonal unit cell with lattice parameters a = 4.1565(1) Å, c = 14.3663(7) Å. Analysis of the extinction indicated only the body-centered Bravais lattice without special conditions. The space group (SG) $I4/mmm$ was chosen for the structure determination. All Th and Pt atoms were located by the direct phase determination procedure (*WinCSD* program package[20]). Since the minor impurity phases ThO_2 (SG $Fm\bar{3}m$, a = 5.5979(2) Å)[30] and $ThPt_3$ always appear in XRD powder patterns of the $ThPt_2$ samples, a multiphase Rietveld refinement was performed. Here it should be noted that we assumed $TiNi_3$ type of structure for the $ThPt_3$ compound on the basis of the indexing of few weak reflections (SG $P6_3/mmc$, a = 5.9103(3) Å, c = 9.7557(6) Å; see Figure 2) and analogy to $ThPd_3$.[31,32] The remaining electronic densities after the final differential Fourier synthesis were 1.07 and −0.87 e^- Å^{-3}, respectively. This, as well as compositions $Th_{0.98(2)}Pt_{2.02(2)}$ and $Th_{0.97(3)}Pt_{3.03(3)}$ derived from the EDXS, indicated no additional atoms in the found structural model of $ThPt_2$. Nevertheless, to exclude the possibility of the incorporation of oxygen in the $ThPt_2$ structure we performed refinements assuming the occupation of 2*a* (0 0 0) or 2*b* (1/2 1/2 0) sites by O atoms, which may be suggested from the related crystal structures, e.g., Eu_4As_2O.[33] In both cases no reasonable Pt−O contacts (always <1.95 Å) and physically

DOI: 10.1021/acs.inorgchem.5b00669
Inorg. Chem. 2015, 54, 6338−6346

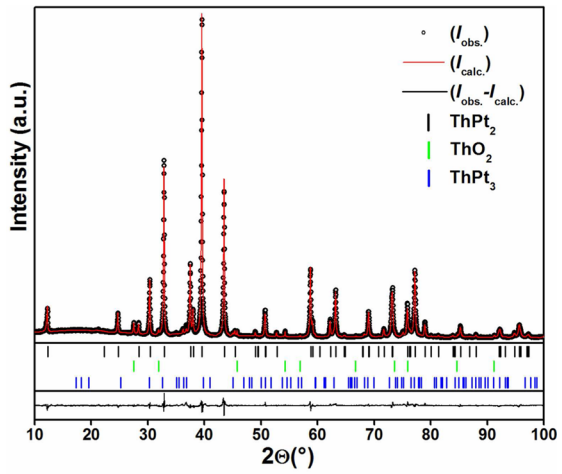

Figure 2. X-ray powder diffraction pattern of $ThPt_2$.

unreasonable displacement parameters for O were obtained. Experimentally observed, theoretically calculated, and differential point intensities, respectively, of the final refinement are shown in Figure 2. Crystallographic details together with final atomic coordinates and displacement parameters for $ThPt_2$ are presented in Tables 1 and 2, respectively, and the interatomic distances as well as coordination numbers of atoms are collected in Table 3. They agree well with sums of atomic radii of elemental Th and Pt (r_{Th} = 1.80 Å; r_{Pt} = 1.38 Å).[42] No shortening is observed for Pt−Pt and Th−Th contacts, while Th−Pt1 and Th−Pt2 distances are shrunk by 3.6% and 7.0%, respectively. This finding agrees well with the charge transfer from Th to Pt observed in a previous XPS study[10] and with the results of the electronic structure calculation and chemical bonding analysis (see below).

Table 1. Crystallographic Data for $ThPt_2$[a] and Hypothetic "Th_2Pt_4O"

	$ThPt_2$	"Th_2Pt_4O"
space group	*I*4/*mmm* (no. 139)	
unit cell params		
a (Å)	4.1565(1)	4.3278
c (Å)	14.3663(7)	14.2818
c/*a*	3.456	3.300
V (Å^3)	248.20(2)	267.5
formula units/cell, *Z*	4	2
calcd density, g/cm^3	16.65(1)	15.65
$2\theta_{max}$ (deg)	100	
N_{hkl} in measured range	57	
radiation, λ (Å)	Cu Kα_1, 1.54056	
step size (deg 2θ)	0.005	
R_I/R_P[a]	0.021/0.112	

[a] $R_I = \sum|I_i^{obs} - I_i^{calc}|/\sum|I_i^{obs}|$; $R_P = \sum w(I_i^{obs} - I_i^{calc})^2/\sum w(I_i^{obs})^2$.

Table 2. Atomic Coordinates and Displacement Parameters for $ThPt_2$ as well as Atomic Coordinates for Hypothetic "Th_2Pt_4O"[a]

atom	site	*y*	*z*	B_{iso}
		$ThPt_2$		
Th	4*e*	0	0.3429(3)	0.44(9)
Pt1	4*c*	1/2	0	0.5(2)
Pt2	4*e*	0	0.1345(3)	0.5(1)
		Th_2Pt_4O		
Th	4*e*	0	0.3371	
Pt1	4*c*	1/2	0	
Pt2	4*e*	0	0.1342	
O	2*b*	0	1/2	

[a] *x* = 0 for all given crystallographic sites.

Table 3. Interatomic Distances *d* (Å) in the Crystal Structure of $ThPt_2$

atoms	*d*, Å	CN
Th		
−4Pt2	2.9570(6)	17
−1Pt2	2.994(5)	
−4Pt1	3.068(3)	
−4Th	3.970(3)	
−4Th	4.1565(1)	
Pt1		
−4Pt2	2.838(3)	12
−4Pt1	2.9391(1)	
−4Th	3.068(3)	
Pt2		
−4Pt1	2.838(3)	9
−4Th	2.9570(6)	
−1Th	2.994(5)	

Crystal Structure Description. The crystal structure of $ThPt_2$ belongs to the variety of tetragonal structures with space group *I*4/*mmm*, unit cell parameters *a* = 4−5 Å; *c* = 14−18 Å and Pearson symbol *tI*12, where atoms occupy three crystallographic sites: 4*c* (0 1/2 0), 4*e*^{1} (0 0∼0.15), and 4*e*^{2} (0 0∼0.35). Additionally, two octahedral voids are formed in such a structural motif with the centers at 2*a* (0 0 0) and 2*b* (0 0 1/2). Since the *c*/*a* ratio in these structures varies in a broad range (3.3−4.3) and all above-mentioned Wyckoff positions can be occupied by diverse sorts of atoms (see Table 4), the experimentally obtained atomic arrangements are claimed in the literature as separate types of structures. The first observed structural representative with such atomic arrangement was Ti_2Bi[34] (general formula T_2X, where T is a transition metal and X is a p element). The La_2Sb structure type[35] (Figure 3) is a representative for a number of A_2X structures with more electropositive elements (A = Ca, Ba, Sr, La−Nd, Sm, Eu and X = P, As, Sb, Bi).[36,37] Later, "Eu_2As" was shown to contain oxygen, which occupies the 2*b* site and thus centers two of the four available octahedral voids in the tetragonal structure.[33] These findings indicated Eu_4As_2O as the actual composition of the compound described now by the general formula $A_8X_4\square_2O_2$ (Table 4, Figure 3). Further studies showed that almost all alkaline-earth metal containing compounds A_2X are stabilized by interstitial oxygen and have indeed a composition A_4X_2O.[37] Only RE_2Sb (RE = rare-earth metal) compounds from this series after extensive theoretical and experimental investigations were confirmed to crystallize with the La_2Sb prototype[37,38] without oxygen inclusion. Two ternary structure types UTeGe ($A_4X_4X'_4$)[39] and CeScSi ($A_4T_4X_4$)[40] also belong to the variety of discussed tetragonal structures (Table 4). On the other hand, the K_2NiF_4 type[41] can be considered as an antitype to the Eu_4As_2O structure, where the X component (fluorine) is occupying the site of the heavier Eu atoms and the position of As is possessed by larger potassium (A component). Also in K_2NiF_4 Ni atoms occupy two octahedral voids with the

DOI: 10.1021/acs.inorgchem.5b00669
Inorg. Chem. 2015, 54, 6338−6346

Table 4. Occupation of the Crystallographic Sites in the Structures Related to the Ti_2Bi Type[a]

	Ti_2Bi	La_2Sb	$ThPt_2$	UTeGe	CeScSi	Eu_4As_2O	K_2NiF_4
	T_8X_4	A_8X_4	A_4T_8	$A_4X_4X'_4$	$A_4T_4X_4$	$A_8X_4\square_2O_2$	$A_4X_8T_2\square'_2$
c/a	3.589	3.909	3.456	4.282	3.674	3.379	3.259
2*a*							Ni
2*b*						O	
4*c*	Ti	La	Pt	Ge	Sc	Eu	F
$4e^{1b}$	Ti	Sb	Pt	U	Si	As	F
$4e^{2b}$	Bi	La	Th	Te	Ce	Eu	K

[a]Space group *I*4/*mmm*. [b]$4e^1$ with atomic coordinates (0 0~0.15) and $4e^2$ with (0 0~0.35), respectively.

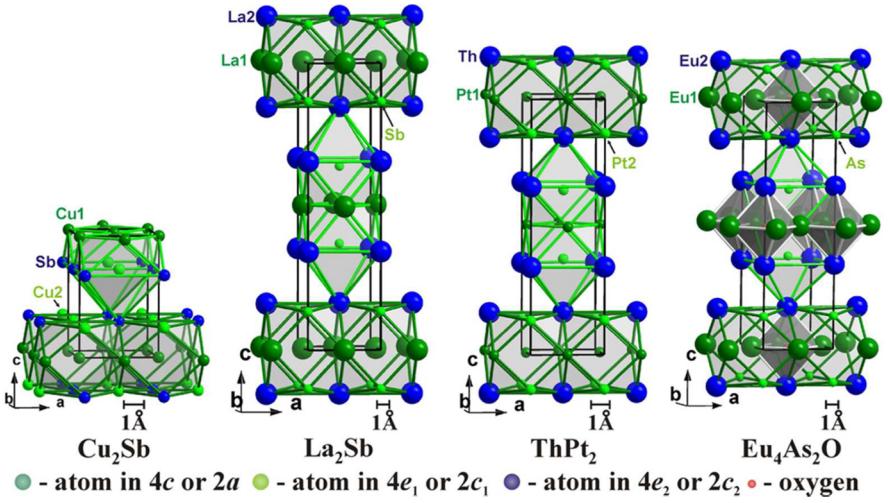

Figure 3. Arrangement of the tetragonal antiprisms (*CN* = 9) and cuboctahedra (*CN* = 12) in the closely related Cu_2Sb, La_2Sb, $ThPt_2$, and Eu_4As_2O structure types. Large balls correspond to f elements, and small balls indicate d (Cu, Pt) or p elements (As, Sb).

centers in 2*a* site indicating a general formula $A_4X_8T_2\square'_2$ for this compound.

Among all the structure types listed in Table 4 and discussed above, $ThPt_2$ is the first representative of such an atomic arrangement without a p element and a formula A_4T_8. It resembles the Ti_2Bi type (Pt atoms occupy the sites of Ti, thus both are d elements), however Th (A component) is now situated at the position of Bi (X component) (Figure 3). This implies that empty octahedra centered at 2*b* (0 0 1/2) in this structure consist now of 4Pt and 2Th while those with the center at 2*a* (0 0 0) are built by 4 Pt1 and 2 Pt2 atoms. In A_2X compounds crystallizing with La_2Sb type, these octahedra are formed by 6 electropositive A atoms. Taking into account the large electronegativity of Pt,[42] the inclusion of oxygen in the octahedra is rather unlikely.

Ti_2Bi and La_2Sb are considered as the superstructures of the Cu_2Sb type (SG *P*4/*nmm*, *a* = 4.0021 Å, *c* = 6.1038 Å)[43,44] with two unit cells (real and mirrored) stacked along the [001] direction[34−36] (Figure 3). Here it should be noted that the Cu_2Sb structure type is based on the ABC close packed structure, where all octahedral and half of the tetrahedral voids are filled by Cu atoms.[45,46] The slabs of condensed cuboctahedra extending in *a* and *b* directions in all compounds presented in Table 4 and Figure 3 are a clear indication of the presence of close packed layers in the studied structure types.

Electronic Structure. The total and partial electronic densities of states (DOS) of $ThPt_2$, computed using a scalar relativistic Hamiltonian, are given in Figure 4. The valence states have the same band width in the fully relativistic calculation. The spin-orbit coupling has a stronger effect on Th

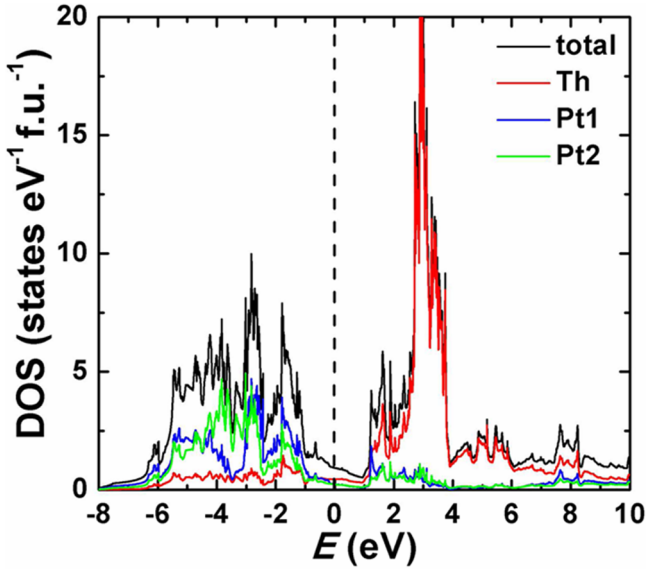

Figure 4. Calculated (scalar relativistic) electronic density of states of $ThPt_2$.

6p states. They are located at −22.7 eV (6p-1/2) and around −15.4 eV (6p-3/2). Although the former is very sharp, the latter has a bandwidth of 0.8 eV. In the scalar relativistic calculation Th 6p states appear around −18 eV (close to the average of the fully relativistic result: [2 × (−22.7) + 4 × (−15.4)]/6 ∼ −17.8 eV). The same feature in the electronic structures is reported for α-$ThSi_2$ and $ThIr_xSi_{2-x}$ (from an XPS study)[47] as well as for ThPtSn.[48] The broad valence band above

DOI: 10.1021/acs.inorgchem.5b00669
Inorg. Chem. 2015, 54, 6338−6346

−8 eV in $ThPt_2$ is mostly formed by Pt 5d states with small contributions of Pt 6s, Th 7s, and Th 6d states (Figure 5b).

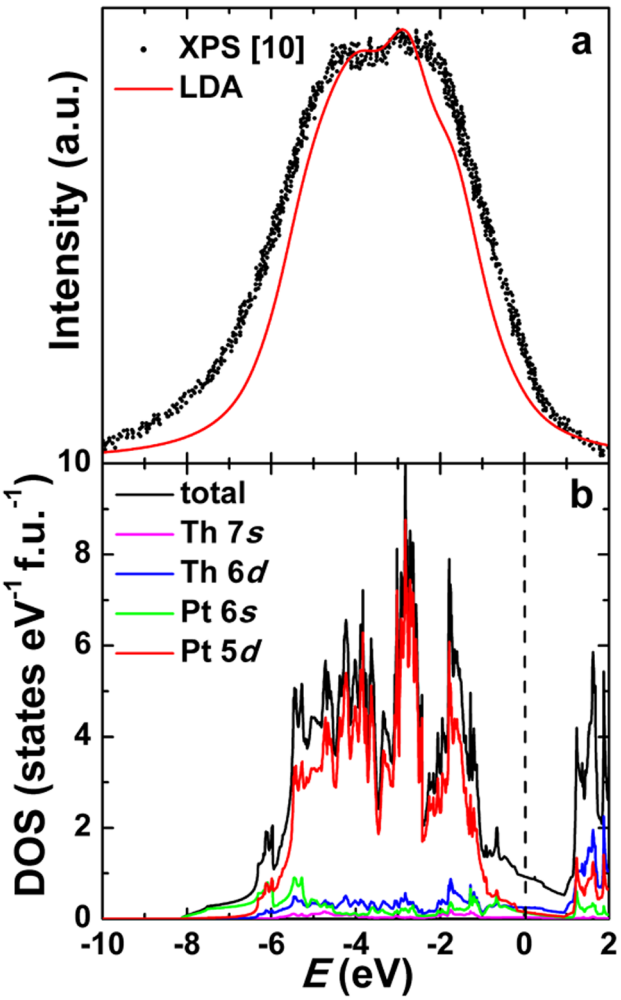

Figure 5. (a) Experimental XPS spectrum of the valence band of $ThPt_2$ excited with Al Kα radiation[10] together with theoretically simulated spectrum from LDA calculation. (b) PDOS, which are mostly contributing to the valence band of $ThPt_2$.

Covalent mixing of the Pt 5d with Th 7s and 6d states observed in our calculation is in excellent agreement with the reported decrease of the Pt 5d emission intensity in ThPt[49] and $ThPt_2$.[10] This was explained by the change in the photoionization cross section which is caused by the hybridization of Pt 5d and Th 7s and 6d orbitals. The analysis of the core-level binding energies in $ThPt_2$ indicated charge transfer from Th to Pt in agreement with the previous experimental studies.[10] As expected, nearly all Th 5f states are lying above the Fermi level. The Fermi level is situated in a dip of the DOS with $N(E_F)$ = 0.9 states eV^{-1} $f.u.^{-1}$, which are mostly due to Pt 5d (25%), Pt 6s (20%), Th 6d (30%), and Th 5f (10%) states. A small contribution of Th 5f to the E_F is also reported in the electronic structure of $ThPt_4Ge_{12}$.[50]

Good agreement is found between our theoretical calculations and the experimental XPS data for $ThPt_2$ with subtracted background[10] (Figure 5a). As one can see from Figure 5b the widths of valence bands of the experimentally obtained and calculated spectra are almost the same. The narrowing of the theoretical band indicates a stronger hybridization of Pt 5d with Th 7s and 6d states.[29] The fine structure of the spectra cannot be compared due to the rather low resolution (1.1 eV) of the XPS measurements.[10]

Cubic $ThPt_2$ ($MgCu_2$ type) vs Tetragonal $ThOs_2$ and $ThIr_2$ ($ThPt_2$ type). In order to relate the tetragonal crystal structure of $ThPt_2$ to other Th-containing phases with 1:2 stoichiometry, we compare it with cubic $ThOs_2$ (a = 7.7050 Å) and $ThIr_2$ (a = 7.6615 Å) Laves phases. A relaxation of the structures of both compounds within LDA leads to the optimized unit cell parameters, DOS at the Fermi level $N(E_F)$, and calculated enthalpies of formation ^fΔH with respect to the elemental crystals which are presented in Table 5. Values of ^fΔH agree well with the enthalpies of formation which were obtained from the calculations based on the thermodynamic models as well as experimental enthalpies for $ThOs_2$ ($^fΔH_{exp}$ = −54 kJ mol^{-1} $atom^{-1}$; $^fΔH_{calc}$ = −55 kJ mol^{-1} $atom^{-1}$) and $ThIr_2$ ($^fΔH_{calc}$ = −90 kJ mol^{-1} $atom^{-1}$) at 1200 °C.[51] Our simulation assuming $MgCu_2$ type of structure for $ThPt_2$ showed that it could be a stable phase if one compares its parameters (see Table 5) with the values found for $ThOs_2$ and $ThIr_2$. Moreover, empirical factors controlling the occurrence of Laves phases (i.e., atomic sizes ratio, position of partner elements in the periodic table, etc.), which were analyzed in ref 52, would rather confirm this finding. However, the experimentally observed tetragonal structure for $ThPt_2$ results in a lower DOS at the Fermi level $N(E_F)$ = 0.9 states eV^{-1} $f.u.^{-1}$ and lower enthalpy of formation ^fΔH = −120.6 kJ mol^{-1} $atom^{-1}$, compared to a hypothetic $MgCu_2$ structural arrangement.

The $ThOs_2$ and $ThIr_2$ compounds assuming tetragonal $ThPt_2$ type of structure have been simulated as well. As one can see from Table 5, their enthalpies of formation are larger (for $ThOs_2$ ^fΔH is even positive) than those observed for the cubic structure. Taking into account this fact as well as the higher DOS at E_F for tetragonal structures compared with the cubic ones, one can conclude that the formation of $ThOs_2$ and $ThIr_2$ with tetragonal $ThPt_2$ type structure is rather unlikely.

Simulation of the Oxygen Inclusion in the $ThPt_2$ Structure. The presence of a ThO_2 as impurity in our sample, as well as the investigations performed on A_2X and A_4X_2O[37] compounds, raise the question about the possible stabilization of the $ThPt_2$ structure by oxygen. The distances □-4Pt1 and □-2Th in the empty octahedra of $ThPt_2$ are 2.0783(1) Å and

Table 5. Theoretically Calculated Unit Cell Parameters, Enthalpies of Formation, and DOS at the Fermi Level for Cubic (c) and Hypothetical Tetragonal (t) Modifications of Compounds ThM_2 (M = Os, Ir, Pt) and Th_2Pt_4O

	$ThOs_2(c)$	$ThIr_2(c)$	$ThPt_2(c)$	$ThOs_2(t)$	$ThIr_2(t)$	$ThPt_2(t)$	Th_2Pt_4O
a, Å	7.623	7.599	7.712	4.0686	4.2134	4.1100	4.3278
c, Å				13.9551	13.1247	14.3851	14.2818
c/a				3.430	3.115	3.500	3.300
^fΔH, kJ mol^{-1} $atom^{-1}$	−24.1	−82.0	−101.3	8.14	−61.7	−120.6	
$N(E_F)$, st. eV^{-1} $f.u.^{-1}$	5.69	6.54	7.19	4.47	1.99	0.92	2.12

DOI: 10.1021/acs.inorgchem.5b00669
Inorg. Chem. 2015, 54, 6338−6346

2.2542(6) Å, respectively. If one would assume occupation of the 2*b* site by oxygen atoms, then the shortening of Th−O contacts would be ∼9%. This is not the case for the A_4X_2O compounds, where A−O distances are mostly larger than the sum of atomic radii.[33,37] To shed more light on a possible stabilization of $ThPt_2$ by oxygen, we performed simulation of the hypothetical "Th_2Pt_4O" structure.

For these purposes an oxygen atom was inserted at the 2*b* site of $ThPt_2$. The lattice parameters for "Th_2Pt_4O" were optimized by looking for the minima in the dependence of energy versus *c*/*a* ratios for different volumes with the further relaxation of atomic coordinates. The final optimized values of lattice parameters and atomic coordinates for "Th_2Pt_4O" are presented in Tables 1 and 2, respectively. As one can see for such structure, a much larger lattice volume compared to $ThPt_2$ is expected. Insertion of oxygen leads also to the reduction of the *c*/*a* ratio in "Th_2Pt_4O" (see Table 1). Both these findings reflect the tendency observed for the series of A_2X and A_4X_2O compounds.[33,37] Also in "Th_2Pt_4O" the contacts Pt−O and Th−O of 2.164 and 2.327 Å become significantly longer than the □-Pt1 and □-Th contacts in the experimentally found $ThPt_2$. These results confirm the reliability of the $ThPt_2$ structural model (Table 2) and render stabilization by interstitial oxygen unlikely.

Chemical Bonding. The interatomic distances in the crystal structure of $ThPt_2$ do not show significant shortening with respect to the sums of the according atomic radii. Such a shortening is often considered as a fingerprint of stronger atomic interactions in the intermetallic compounds. Therefore, in order to shed more light on the organization of the crystal structure of $ThPt_2$ in comparison with chemically related intermetallic compounds and on the reasons of such structural behavior, chemical bonding in $ThPt_2$ was studied by means of the combined analysis of electron density and electron localizability indicator.[25,53,54]

Application of the quantum theory of atoms in molecules (QTAIM)[55] on the calculated electron density in $ThPt_2$[27] reveals significant charge transfer from Th to the Pt atoms (Figure 6, top panel), as expected from the difference in the Pauling electronegativity of the elements: EN(Pt) = 2.28, EN(Th) = 1.3.[42] Being in agreement with different coordination, Pt2 anions—basins of which have common surface with the five thorium basins, and the Th−Pt2 distances are shorter than that of Th−Pt1—show larger negative charge in comparison with the Pt1, that have a common surface with four neighboring Th atoms and longer Th−Pt distances.

Distribution of the electron localizability indicator reveals strong structuring of the penultimate atomic shells of Th and Pt (Figure 6, middle panel), if compared with the spherical distribution for isolated atoms of thorium and platinum. Such redistribution of ELI-D is a fingerprint of the participation of these electrons in the bonding within the valence region.[26,56] The interaction between platinum atoms (Figure 6, middle panel) appears not as an attractor (cf. Cu−Cu[57]) but as the structuring of the penultimate shells, manifested for both participating atoms by lower ELI-D values at the ring point located close to the direct line connecting the nuclei (a "hole" in the penultimate shell). Four ELI-D maxima are located around the shortest Th−Pt2 contact (Figure 6, middle panel) resembling a ring attractor, found for the transition-metal−p element and transition-metal−transition-metal interaction in the molecular model systems (cf. Sc−Ga,[56] $(Sc−Sc)^{2+}$ [refs 56 and 61], and Cu−Cu[57]). Such attractor suggests a direct Th−

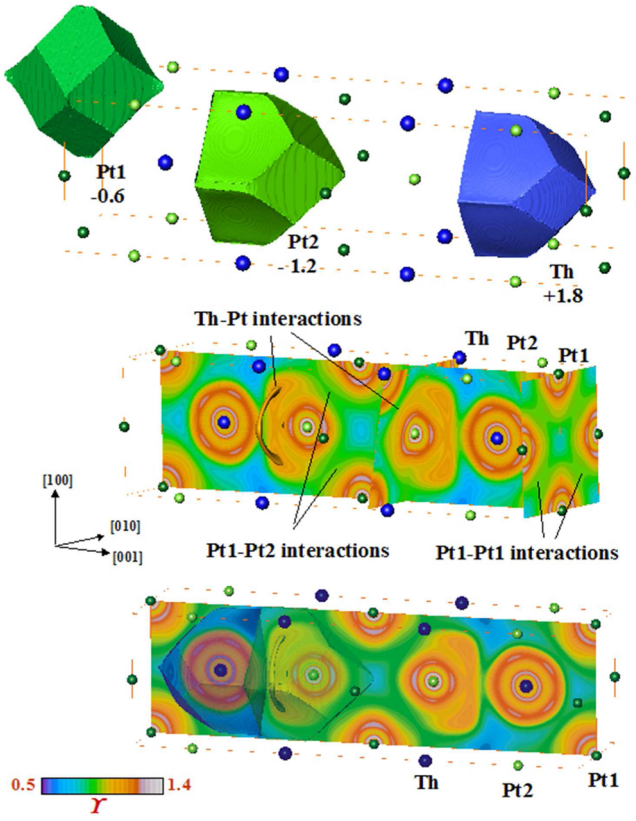

Figure 6. Chemical bonding in $ThPt_2$: (top panel) shape and effective charge of the atomic basins (QTAIM atoms); (middle panel) ELI-D distribution in the planes at $x = 0.5$, $z = 0.0$ and $z = 0.343$ and isosurface with $\Upsilon = 1.08$ in the region between Th and Pt2 atoms; (bottom panel) intersection of the QTAIM atoms (transparent shapes) and the ELI-D distribution revealing the location of the ELI-D maxima within the atomic basin of Pt2.

Pt2 bonding in $ThPt_2$. The ELI-D attractors reflecting this Th−Pt2 interaction are located within the atomic basin of Pt (Figure 6, bottom panel). Further analysis applying the intersections technique[59] reveals that 82% of the charge in this basin belongs to the QTAIM basin of Pt2, 12% to the neighboring four equivalent Pt2 basins, and only 6% originates from the QTAIM basin of Th. Thus, this Th−Pt2 interaction should be considered as a (strongly) polar one. On the other hand, the ELI-D distribution around the second long Th−Pt2 contact (see Table 3) does not show dedicated attractors in this region. Instead it reveals characteristic structuring of the penultimate shells visualizing in this way a Th−Pt2 interaction different from the former Th−Pt2 one.

The evolution of metal (*M*)−platinum and platinum−platinum interactions in dependence of the number of valence electrons available in MPt_2 compounds with *M* = Na, Ba, Ce, and Hf is illustrated in Figure 7. The second shell of Na in $NaPt_2$ (structure type of the Laves phase $MgCu_2$, Figure 7 top) has spherical shape as expected for a $2s^22p^6$ configuration. The outer (3rd) shell of sodium is not present being in agreement with predominantly ionic interaction between sodium and the platinum polyanion, similarly to other Laves phases with alkali metals[58] and with a large electronegativity difference between Na and Pt. In addition to that, local maxima of ELI-D are observed on the lines between Na and Pt, being located within the penultimate shells of Pt atoms. Finally, dedicated ELI-D maxima are found on the Pt−Pt contacts revealing the covalent

DOI: 10.1021/acs.inorgchem.5b00669
Inorg. Chem. 2015, 54, 6338−6346

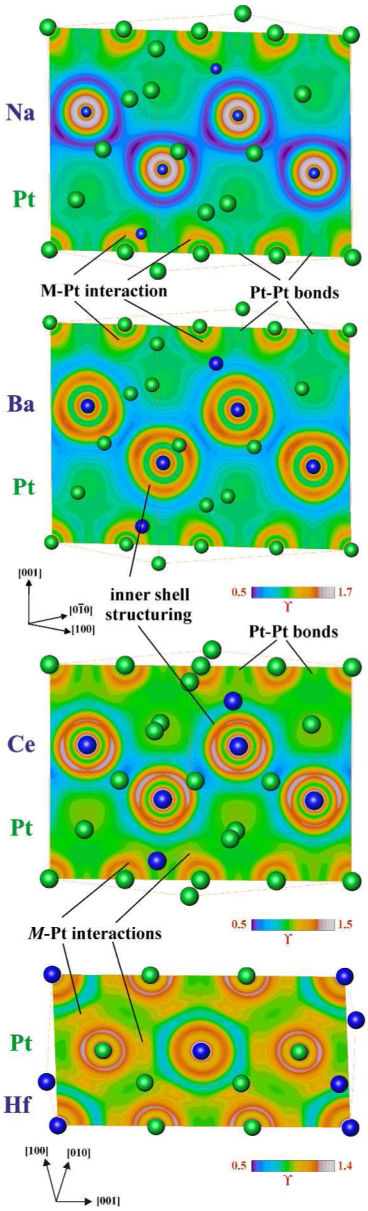

Figure 7. Chemical bonding in MPt_2 compounds in the ELI-D representation: $NaPt_2$ (top panel), $BaPt_2$ (middle upper panel), $CePt_2$ (middle lower panel) and $HfPt_2$ (bottom panel). The ELI-D distribution in characteristic planes is shown, which contain both M−Pt and Pt−Pt contacts. The topology evolution of ELI-D distribution on the Pt−Pt and M−Pt contacts as well as structuring of the penultimate shells of the M atoms changes systematically with the number of the valence electrons available, being less sensitive to the structural pattern.

interaction within the anionic platinum substructure. In the barium-containing Laves phase $BaPt_2$ (structure type $MgCu_2$), the Pt−Pt interactions are also indicated by the dedicated ELI-D maxima on the according contact lines (Figure 7, middle upper panel). The structuring of the penultimate shell of Ba is here clearly pronounced in comparison with $NaPt_2$. The shell has a shape which deviates from the spherical one expected for the completely ionic behavior of Ba. The ELI-D maxima on the Ba−Pt lines become also more pronounced. The evolution toward a more pronounced structuring and deformation of the penultimate shell continues if considering the Laves phase $CePt_2$ (structure type $MgCu_2$, Figure 7, middle lower panel). In this way the *M*−Pt interaction earns more and more covalent (polar) character moving away from the ionic one, which is within the general tendency of bonding changes in Laves phases.[58] Replacement of Ce by Hf leads to formation of a new structural pattern for the MPt_2 compounds, namely, one of the $MoSi_2$ type (at the non-stoichiometric composition $Hf_{1.2}Pt_{1.8}$[60]). The atomic arrangement in $HfPt_2$ is more similar to that in $ThPt_2$ than to the Laves phases (cf. Figures 6 and 7). Both crystal structures—$HfPt_2$ and $ThPt_2$—are characterized by similar atomic layers perpendicular to [001]. In the ideal crystal structure of $HfPt_2$, the Pt−Pt interactions show the structuring of the penultimate shells in the ELI-D distribution, similarly to the situation in $ThPt_2$ (Figure 7, bottom). The Hf−Pt interactions are revealed by ELI-D attractors between the Pt and Hf cores, and may be understood as the next step of the bonding evolution toward $ThPt_2$, where the similar Th−Pt2 interaction is visualized by a ring-like superbasin in ELI-D distribution. The QTAIM charges in the MPt_2 compounds investigated are presented in Table 6. In agreement with the

Table 6. QTAIM Charges in MPt_2 Compounds

	effective QTAIM charge			
compound	M	Pt	normalized effective QTAIM charge on Pt[a]	electronegativity difference EN(Pt) − EN(M)[b]
$NaPt_2$	+0.78	−0.39	−0.39	0.43
$SrPt_2$	+1.32	−0.66	−0.33	0.45
$BaPt_2$	+1.20	−0.60	−0.30	0.47
YPt_2	+1.60	−0.80	−0.27	0.38
$LaPt_2$	+1.42	−0.71	−0.24	0.36
$CePt_2$	+1.36	−0.68	−0.23	0.36
$ThPt_2$	+1.78	−1.22	−0.41 (av)	0.33
		−0.59	−0.20 −0.30	
$HfPt_2$	+1.76	−0.88	−0.22	0.19

[a]Effective QTAIM charge of Pt divided by the formal number of valence electrons of M according to its position in the Periodic Table. [b]Allred−Rochow scale.

electronegativity differences, a charge transfer from *M* to Pt is observed. In order to compare different MPt_2 compounds, the normalization of the charge transfer per Pt atom was performed using the formal number of valence electrons of *M* (one for Na, two for Sr and Ba, three for Y, La, Ce, and Th, and four for Hf). The so-normalized charge transfer is found to be proportional to the electronegativity difference between the components, showing a similar trend recently found for Laves phases.[58] Thus, the appearance and manifestation of the polar *M*−Pt and non-polar Pt−Pt interactions in MPt_2 compounds are consistent with the electronegativity difference between the components.

Summarizing, the bonding organization in $ThPt_2$ can be understood as formation of a three-dimensional framework by two-center interactions. The framework consists of Pt layers with vertex-sharing Pt_6 octahedra in the (001) plane (centered at 2*a* site (1/2 1/2 1/2)). The (001) plane interaction (shorter contact) involves a (strongly) polar ring attractor and the interaction along the [001] (longer contact) manifests itself in the form of penultimate shell structuring.

Physical Properties. The magnetic susceptibility of $ThPt_2$ is negative with a weak positive linear temperature dependence and an upturn at low temperature caused by minor paramagnetic impurities (Figure 8). The extrapolated χ_0 at $T = 0$ K

DOI: 10.1021/acs.inorgchem.5b00669
Inorg. Chem. 2015, 54, 6338−6346

is -9.35×10^{-5} emu mol^{-1}. No superconductivity or other phase transitions were observed for $ThPt_2$ down to 1.8 K in fields of $\mu_0 H \geq 2$ mT.

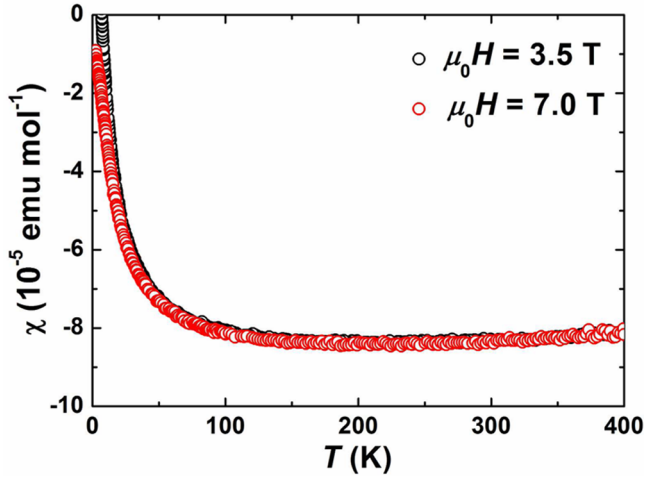

Figure 8. Magnetic susceptibility of $ThPt_2$ in different magnetic fields.

The electrical resistivity, $\rho(T)$, of polycrystalline $ThPt_2$ increases with increasing temperature in the whole measured temperature range and is rather small (Figure 9). No

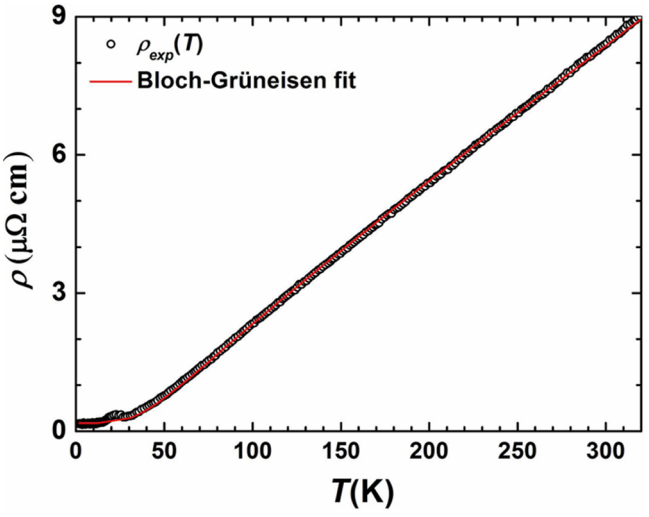

Figure 9. Electrical resistivity of $ThPt_2$ together with the fit to the Bloch–Grüneisen law.

superconductivity is observed down to 0.35 K. Electrical resistivity can be successfully fitted to a modified Bloch–Grüneisen relation in the temperature range 1.8–320 K with the values of residual resistivity $\rho_0 = 0.17$ $\mu\Omega$ cm, parameter $A_{BG} = 2.8 \times 10^{-2}$ $\mu\Omega$ cm K^{-1}, and Debye temperature $\theta_D = 226$ K, in good agreement with $\theta_D(0) = 232$ K from specific heat (see below). All these findings indicate typical metallic behavior of $ThPt_2$. The room-temperature resistivity $\rho_{(300K)}$ of $ThPt_2$ of 8.2 $\mu\Omega$ cm together with the small ρ_0 indicates a good quality of the investigated specimen (RRR = 48). The anomaly observed in $\rho(T)$ at ~23 K is a measurement artifact, which appears due to the low resistivity of $ThPt_2$.

The molar heat capacity $c_p(T)$ of $ThPt_2$ is given in the inset of Figure 10. The value of 77.5 J mol^{-1} K^{-1} observed at 298 K

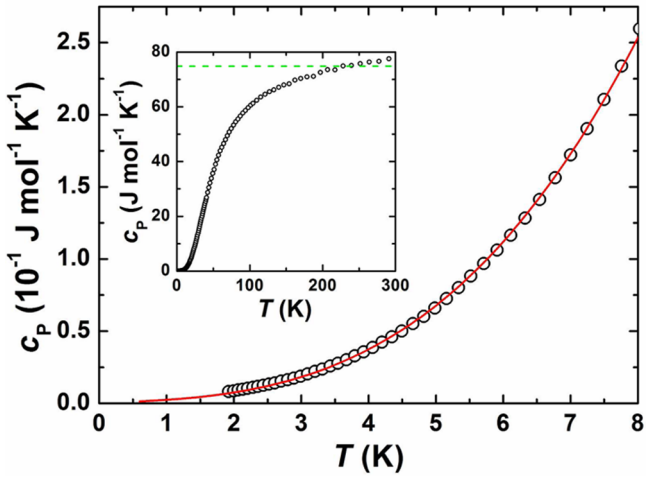

Figure 10. Low-temperature specific heat $c_p(T)$ for $ThPt_2$ (black circles) together with the fit to the $c_p(T) = \gamma T + \beta T^3$ equation for $T <$ 8 K (red line) (see text). The inset shows the molar heat capacity of $ThPt_2$ in the whole studied temperature range (1.8–300 K) with Dulong–Petit limit (green dashed line).

for the compound agrees well with the Dulong–Petit limit ($c_p \approx 3nR$, where n is the number of atoms per f.u.). The low-temperature specific heat of $ThPt_2$ for $T < 8$ K (Figure 10) can be described by $c_p(T) = \gamma T + \beta T^3$, where γ is the Sommerfeld coefficient of the electronic heat capacity, and β is the Debye approximation for the phonon contribution. A fit with the simple relation above (see red line in Figure 10), in the temperature range 1.8–8 K, results in $\gamma = 1.9$ mJ mol^{-1} K^{-2} and $\beta = 4.7 \times 10^{-4}$ J mol^{-1} K^{-4}, corresponding to an initial Debye temperature $\theta_D(0) = 232$ K. The small value of γ indicates a low DOS at the Fermi level of ≈0.8 state eV^{-1} f.u.$^{-1}$ and metallic properties of $ThPt_2$, which is in agreement with the theoretical calculations.

CONCLUSIONS

The crystal structure of $ThPt_2$ is the first representative of tetragonal close packed structures (Pearson symbol *tI*12) without p element. Calculations of the electronic structure of $ThPt_2$ indicate strong hybridization of Pt 5d and Th 7s and 6d orbitals and electron transfer from Th to Pt. In line with this, the bonding analysis by electron localizability approach reveals the three-dimensional framework structure of $ThPt_2$ to consist of a two-dimensional anionic platinum substructure being separated by the positively charged Th species, whereby the Th–Pt interaction shows strongly polar covalent character. The appearance and manifestation of the polar *M*–Pt and nonpolar Pt–Pt interactions in $ThPt_2$ and other MPt_2 compounds (*M* is a more electropositive metal) are consistent with the electronegativity difference between the components. Theoretical simulations show lower enthalpy of formation $^f\Delta H = -120.6$ kJ mol^{-1} atom^{-1} for the tetragonal crystal structure of $ThPt_2$ compared to $^f\Delta H_{calc} = -101.3$ kJ mol^{-1} atom^{-1} for a possible $MgCu_2$ structural arrangement. Simulation of the fictitious "Th_2Pt_4O" renders stabilization of $ThPt_2$ by interstitial oxygen unlikely. $ThPt_2$ is diamagnetic and shows a metallic type of the temperature dependence of electrical resistivity. No superconductivity is observed for this compound down to 0.35 K. The small value of Sommerfeld coefficient of the electronic heat capacity γ indicates a low DOS at the Fermi level of ≈0.8 state eV^{-1} f.u.$^{-1}$ and metallic properties of $ThPt_2$, which is in

DOI: 10.1021/acs.inorgchem.5b00669
Inorg. Chem. 2015, 54, 6338–6346

agreement with the theoretical calculations ($N(E_F)$ = 0.9 states eV^{-1} f.u.$^{-1}$).

AUTHOR INFORMATION

Corresponding Author

*E-mail: roman.gumeniuk@physik.tu-freiberg.de. Fax: +49 3731 39 4314.

Notes

The authors declare no competing financial interest.

ACKNOWLEDGMENTS

The authors are grateful to L. Akselrud, O. Janson, D. Kasinathan, K. Koepernik, and A. Efimova for fruitful discussions.

REFERENCES

(1) Wernick, J. H. In *Intermetallic Compounds*; Westbrook, J. H., Ed.; Wiley: New York, NY, 1967.
(2) Johnston, R. L.; Hoffmann, R. *Z. Anorg. Allg. Chem.* **1992**, *616*, 105−120.
(3) Sinha, A. K. *Progr. Mater. Sci.* **1972**, *15*, 79−185.
(4) Villars, P. *Pearson's Handbook, Crystallographic Data for Intermetallic Phases*; ASM International: Materials Park, OH, 1997; Vol. *1*.
(5) Zhu, J. H.; Liu, C. T.; Pike, L. M.; Liaw, P. K. *Metall. Mater. Trans. A* **1999**, *30*, 1449−1452.
(6) Eriksson, O.; Johansson, B.; Brook, M. S. S.; Skriver, H. L. *Phys. Rev. B* **1989**, *40*, 9519−9528.
(7) Trainor, R. J.; Brodsky, M. B.; Culbert, H. V. *Phys. Rev. Lett.* **1975**, *34*, 1019−1022.
(8) Dwight, A. E.; Downey, J. W.; Conner, R. A., Jr. *Trans. Am. Inst. Min., Metall. Pet. Eng.* **1958**, *212*, 337−338.
(9) Matthias, B. T.; Compton, V. B.; Corenzwit, E. *J. Phys. Chem. Solids* **1961**, *19*, 130−133.
(10) Schneider, W.-D.; Laubschat, C. *Phys. Rev. B* **1981**, *23*, 997−1005.
(11) Thomson, J. R. *Nature* **1961**, *189*, 217.
(12) Thomson, J. R. *Acta Crystallogr.* **1962**, *15*, 1308−1309.
(13) Thomson, J. R. *Acta Crystallogr.* **1963**, *16*, 320−321.
(14) Thomson, J. R. *J. Less-Common Met.* **1964**, *6*, 3−10.
(15) Peterson, D. E. *Bull. Alloy Phase Diagrams* **1990**, *11*, 237−239.
(16) Erdmann, B.; Keller, C. *J. Solid State Chem.* **1973**, *7*, 40−48.
(17) Geballe, T. H.; Matthias, B. T.; Compton, V. B.; Corenzwit, E.; Hull, G. W., Jr.; Longinotti, L. D. *Phys. Rev.* **1965**, *137*, A119−A127.
(18) Hill, H. H.; Elliot, R. O. *Phys. Lett.* **1971**, *35A*, 73−74.
(19) WinXPow (version 2), Darmstadt, STOE and Cie GmbH, 2001.
(20) Akselrud, L.; Grin, Yu. *J. Appl. Crystallogr.* **2014**, *47*, 803−805.
(21) Leithe-Jasper, A.; Bormann, H.; Hönle, W. Scientific report of MPI CPfS, Dresden, 2003−2005, 24−27.
(22) Jepsen, O. B., Burkhardt, A.; Andersen, O. K. *The Program TB-LMTO-ASA. Version 4.7*; Max-Planck-Institut für Festkörperforschung: Stuttgart, 1999.
(23) Koepernik, K.; Eschrig, H. *Phys. Rev. B* **1999**, *59*, 1743−1757.
(24) Perdew, J. P.; Wang, Y. *Phys. Rev. B* **1992**, *45*, 13244−13249.
(25) Kohout, M. *Int. J. Quantum Chem.* **2004**, *97*, 651−658.
(26) Kohout, M.; Wagner, F. R.; Grin, Yu. *Theor. Chem. Acc.* **2008**, *119*, 413−420.
(27) Kohout, M. Program DGrid, Version 4.6; Radebeul, 2010.
(28) Yeh, J. J.; Lindau, I. *At. Data Nucl. Data Tables* **1985**, *32*, 1−155.
(29) Samsel-Czekała, M.; Troć, R.; Talik, E. *J. Alloys Compd.* **2008**, *451*, 448−449.
(30) Idiri, M.; Le Bihan, T.; Heathman, S.; Rebizant, J. *Phys. Rev. B* **2004**, *70*, 014113.
(31) Thomson, J. R. *Adv. X-Ray Anal.* **1963**, *6*, 91−95.
(32) Dwight, A. E.; Downey, J. W.; Conner, R. A., Jr. *Acta Crystallogr.* **1961**, *14*, 75−76.
(33) Wang, Yu.; Calvert, L. D.; Gabe, E. J.; Taylor, J. B. *Acta Crystallogr.* **1977**, *33*, 3122−3125.
(34) Auer-Welsbach, H.; Nowotny, H.; Kohl, A. *Monatsh. Chem.* **1958**, *89*, 154−159.
(35) Stassen, W. N.; Sato, M.; Calvert, L. D. *Acta Crystallogr.* **1970**, *26*, 1534−1540.
(36) Pearson, W. B. *Z. Kristallogr.* **1985**, *171*, 23−39.
(37) Nuss, J.; Wedig, U.; Jansen, M. *Z. Anorg. Allg. Chem.* **2011**, *637*, 1975−1981.
(38) Nuss, J.; von Schnering, H.-G.; Grin, Yu. *Z. Anorg. Allg. Chem.* **2004**, *630*, 2287−2291.
(39) Haneveld, A. J. K.; Jellinek, F. *J. Less-Common Met.* **1969**, *18*, 123−129.
(40) Mokra, I. R.; Bodak, O. I. *Dopov. Akad. Nauk Ukr. RSR* **1979**, *41*, 312−315.
(41) Baltz, D.; Plieth, K. *Z. Elektrochem.* **1955**, *59*, 545−551.
(42) Emsley, J. *The Elements*; Clarendon Press: Oxford, 1998.
(43) Westgren, A.; Hägg, G. *Z. Phys. Chem.* **1929**, *B4*, 453−468.
(44) Nuss, J.; Jansen, M. *Z. Anorg. Allg. Chem.* **2002**, *628*, 1152−1157.
(45) Krypiakevych, P. *Structure types of intermetallic compounds*; Nauka: Moscow, 1977.
(46) O'Keeffe, M.; Hyde, B. G. *Crystal Structures*; Mineralogical Society of Amerika, BookCrafters, Inc.: Chelsea, 1996.
(47) Chevalier, B.; Zhong, W. X.; Buffat, B.; Etourneau, J.; Hagenmuller, P.; Lejay, P.; Porte, L.; Duc, T. M.; Besnus, M. J.; Kappler, J. P. *Mater. Res. Bull.* **1986**, *21*, 183−194.
(48) Szajek, A.; Morkowski, J. A.; Bajorek, A.; Chełkowska, G.; Troć, R. *J. Magn. Magn. Mater.* **2004**, *281*, 281−289.
(49) Schneider, W.-D.; Laubschat, C. *Phys. Lett. A* **1980**, *75*, 407−408.
(50) Galvan, D. H. *J. Supercond. Novel Magn.* **2009**, *22*, 367−371.
(51) Kleykamp, H. *J. Less-Common Met.* **1979**, *63*, P25−P33.
(52) Dwight, A. E. *Trans. Am. Soc. Met.* **1961**, *53*, 479−500.
(53) Kohout, M. *Faraday Discuss.* **2007**, *135*, 43−54.
(54) Kohout, M.; Wagner, F. R.; Grin, Yu. *Int. J. Quantum Chem.* **2006**, *106*, 1499−1507.
(55) Bader, R. F. W. *Atoms in molecules*; Oxford University Press: Oxford, 1990.
(56) Kohout, M.; Wagner, F. R.; Grin, Yu. *Theor. Chem. Acc.* **2002**, *108*, 150−156.
(57) Grin, Yu.; Wagner, F. R.; Armbrüster, M.; Kohout, M.; Leithe-Jasper, A.; Schwarz, U.; Wedig, U.; von Schnering, H.-G. *J. Solid State Chem.* **2006**, *179*, 1707−1719.
(58) Ormeci, A.; Simon, A.; Grin, Yu. *Angew. Chem., Int. Ed.* **2010**, *49*, 8997−9001.
(59) Raub, S.; Jansen, G. *Theor. Chem. Acc.* **2001**, *106*, 223−232.
(60) Schubert, K.; Raman, A.; Rossteutscher, W. *Naturwissenschaften* **1964**, *51*, 506−507.
(61) Wagner, F. R.; Bezugly, V.; Kohout, M.; Grin, Yu *Chem.—Eur. J.* **2007**, *13*, 5724−5741.

DOI: 10.1021/acs.inorgchem.5b00669
Inorg. Chem. 2015, 54, 6338−6346